Physics of U.S. surface temperature response to ENSO

Tao Zhang, Martin P. Hoerling, Judith Perlwitz,

De-Zheng Sun, and Don Murray

Cooperative Institute for Research in Environmental Sciences

University of Colorado/NOAA Earth System Research Laboratory

Physical Sciences Division

Boulder, Colorado

(*Submitted to Journal of Climate*)

December 17, 2010

(Revised)

Corresponding author address: Dr. Tao Zhang, 325 Broadway, R/PSD1, CIRES and NOAA/PSD, Boulder, CO 80305. Email: tao.zhang@noaa.gov

Abstract

In order to elucidate physical processes responsible for the U.S. response to El Niño/Southern Oscillation (ENSO), the surface energy balance is diagnosed from observations with emphasis on the role of clouds, water vapor, and land surface properties associated with snow cover and soil moisture. Results for the winter season (December, January, February) indicate that U.S. surface temperature conditions associated with ENSO are determined principally by anomalies in the surface radiative heating—the sum of absorbed solar radiation and downward longwave radiation. Each component of the surface radiative heating is linked with specific characteristics of the atmospheric hydrologic response to ENSO, and also to feedbacks by the land surface response. During El Niño, surface warming over the northern U.S. is physically consistent with three primary processes: i) increased downward solar radiation due to reduced cloud optical thickness, ii) reduced reflected solar radiation due to an albedo decline resulting from snow cover loss, and iii) increased downward longwave radiation linked to an increase in precipitable water. In contrast, surface cooling over the southern U.S. during El Niño is mainly the result of a reduction in incoming solar radiation resulting from increased cloud optical thickness. During La Niña, surface warming over the central U.S. results mainly from snow cover losses, whereas warming over the southern U.S. results mainly from a reduction in cloud optical thickness which yields increased incoming solar radiation, and also from an increase in precipitable water which enhances the downward longwave radiation. For both phases of ENSO the surface radiation budget is closely linked to large-scale horizontal and vertical motions in the free atmosphere via two main processes: i) the convergence of the atmospheric water vapor

transport which largely determines cloud optical thickness and thereby affects incoming shortwave radiation, and ii) the changes in tropospheric column temperature resulting from the characteristic atmospheric teleconnections which largely determine column precipitable water and thereby affect downward longwave radiation.

1. Introduction

El Niño-Southern Oscillation (ENSO) induces a strong natural interannual climate signal that affects the surface climate in numerous regions of the globe including the continental United States. The effect of ENSO on the U.S. surface temperature has been documented in many previous studies (Ropelewski and Halpert, 1986, 1987; Kiladis and Diaz 1989; Hoerling et al. 1997; Larkin and Harrison 2005; Wang et al. 2007; Lau et al. 2008). During El Niño winter, the northern contiguous United States is dominated by warm temperature anomalies and the southern United Sates is dominated by cold temperature anomalies. During La Niña winter, there is a general reversal in temperature anomalies in many regions of the United States, though the response is not strictly linear (e.g. Hoerling et al. 1997). Despite the strong impact of ENSO on U.S. climate and even though it is widely recognized to provide the principal source of seasonal forecast skill for the U.S. (e.g. Quan et al. 2006), little is known about the physical processes responsible for the surface temperature signals. Virtually all of ENSO-impact studies have focused on atmospheric teleconnections (e.g. Trenberth et al. 1998; Hoerling and Kumar 2000), but these alone can not explain the immediate causes for the surface temperature anomalies.

At the surface, temperature changes are determined by diabatic heating which is intimately tied to the hydrological cycle including the radiative effects of water vapor, clouds and changes in surface properties such as soil moisture and snow cover. It is understood that the tropical SST anomalies excite the propagation of Rossby waves from the tropical Pacific polewards and eastwards to the Americas and thereby affect the

region's climate (see review by Trenberth et al. 1998). An open question is how circulation anomalies modify water vapor, clouds and land surface properties over the Americas because these changes are critical for the surface energy balance that determines the characteristics of surface temperature responses to ENSO.

As an essential component of the global hydrologic cycle, water vapor and clouds contribute significantly to Earth's climate (e.g. Chahine 1992; Ramanathan et al. 2001; Sun et al. 2003). While extensive efforts have been devoted to assessing the changes in the hydrologic cycle associated with ENSO over the oceans (Soden 2000; Sun et al. 2003, 2006, 2009; Zhang and Sun 2006, 2008), less attention has been given to describing the changes in the hydrologic cycle over land, especially over the continental United States. Yang et al. (2001) studied the impact of snow variability induced by ENSO on surface temperature responses over the North America. Their results indicated that the snow-albedo feedback is an important factor affecting the North America surface climate anomaly. Snow-albedo feedback effects constitute only one component of local surface diabatic heating however, namely the upward shortwave radiative flux at the surface. The role of water vapor and clouds, which control the downward longwave and downward shortwave radiative fluxes, remains to be understood.

The purpose of this paper is to understand the physics of U.S. surface temperature response to ENSO by highlighting the role of water vapor, clouds and land surface interactions. Section 2 describes the methodology and the observational datasets used in this study. Section 3 first presents the observed composite anomalies of U.S. surface

temperature during El Niño and La Niña, and then illustrates the composite surface energy components that maintain the U.S. surface temperature patterns. The relative roles of water vapor, clouds and snow cover are examined in order to understand the physical processes underlying the various surface energy fluxes. A summary of principal results is given in section 4 where we interpret the surface temperature anomalies during ENSO within a holistic framework that integrates the immediate effects of physical processes inherent in the energy balance with the ultimate causal effects linked to the free atmospheric teleconnections.

2. Methodology and Data

The surface energy balance is subject to the law of energy as indicated in equation (1):

$$Cs\frac{\partial T}{\partial t}=\Delta SW_{absorbed}+\Delta LW_{down}+\Delta LW_{up}+\Delta SH+\Delta LH+\Delta GH+\Delta M\ , \qquad (1)$$

where Cs is the surface layer heat capacity per unit area, $\frac{\partial T}{\partial t}$ is the temperature tendency, $SW_{absorbed}$, LW_{down}, and LW_{up} are the absorbed shortwave radiative flux at surface, downward and upward longwave radiative fluxes at surface, respectively, SH and LH are the sensible and latent heat fluxes, GH is the ground heat flux and M is the energy flux used for melt.

As demonstrated by Wild et al. (2004), the last two terms (ΔGH and ΔM) are negligible, and for the time-averaged states considered here, the temperature tendency is also effectively zero. Thus the surface energy balance that maintains the surface temperature distribution is given by

$$\Delta SW_{absorbed} + \Delta LW_{down} + \Delta LW_{up} + \Delta SH + \Delta LH = 0. \qquad (2)$$

The sum of the absorbed shortwave and downward longwave radiation fluxes (the first two terms of Equation (2)) is defined as the surface radiative heating, which indicates the radiative energy input to the surface. In response to the imposed change of surface radiative heating, the surface redistributes the changed energy content among the non-radiative fluxes of the surface energy balance (SH and LH) and the surface longwave emission (LW_{up}).

In the present study, we focus on the impact of ENSO on the U.S. hydrologic cycle during Northern winter (December to February) using multiple observational datasets. We conduct composite analysis to understand coherent features in the response of the hydrologic cycle to El Niño and La Niña SST forcing over the continental United States. The definition of warm and cold events is based on the same method as used by Hoerling et al. (1997), and the warm and cold event years used in the composite (see Table 1) are selected due to the availability of the satellite data from which to determine the surface energy balance.

The ISCCP (International Satellite Cloud Climatology Project) FD data (Zhang et al. 2004) and ISCCP D2 data (Rossow et al. 1996) are used for examining the response of water vapor and clouds over the U.S. to ENSO forcing, respectively. The ISCCP FD data also include the monthly radiative fluxes both at surface and at the top of the atmosphere (TOA), which allows us to perform the surface energy budget analysis. The corresponding surface latent and sensible heat fluxes are obtained from ERA-40 reanalysis (Uppala et al. 2005). For consistency, the surface temperature data from

ISCCP FD data sets are also used in this study. We examine the responses of snow cover and soil moisture from North American Regional Reanalysis (NARR) data (Mesinger et al. 2006) to infer features of land surface wetness over the continental United States, and analyze the CMAP precipitation (Xie and Arkin 1997) data to infer soil moisture conditions.

The air temperature from NCEP/NCAR reanalysis (Kalnay et al. 1996) and the vertically integrated water vapor transport (Trenberth, 1997) are used to understand the link between the large-scale dynamics and the local impacts of water vapor and clouds. ERA-40 reanalysis data is used to estimate the composite anomalies for sensible and latent heating instead of NARR data, because we found that ERA-40 data has a better spatial agreement in net radiation with ISCCP data compared to NARR data. In addition, the corresponding turbulent fluxes in ERA-40 exhibit a better compensation with ISCCP net radiation, compared to NARR turbulent fluxes.

Our analysis is based on 6 warm and 4 cold events. This relatively small sample size results from the brevity of the satellite observations available from which we can calculate the surface energy balance. Because standard t-statistics can be very unreliable in estimating the statistical significance of the response when the sample is small, we determined the robustness of our estimates by calculating the "sign agreement" for key physical components of the surface radiation budget.

3. Results

3.1. Composite Surface Temperature Anomalies

The wintertime patterns of the surface temperature anomalies observed during El Niño and La Niña are displayed in the top and bottom panels of Figure 1, respectively. During El Niño, maximum warm temperature anomalies are located over western Canada and the northern U.S., while the surface temperature is colder than normal over the southern and eastern tiers of the U.S. (Figure 1a). These key features agree well with the previous observational findings based on larger sample sizes (e.g. Hoerling et al. 1997; Larkin and Harrison 2005; Lau et al. 2008).

There is a general reversal in the pattern of surface temperature anomalies during La Niña, with the cold (warm) anomalies prevailing in the northwest (southeast) of the North American landmass (Figure 1b). The present composites for ENSO events after 1986 show an asymmetry in temperature anomalies over the northern regions of U.S. (about poleward of 37^{o}N), where strong warm anomalies occur during both El Niño and La Niña events, consistent with a nonlinearity in ENSO teleconnections reported in Hoerling et al. (1997).

3.2 Composite Surface Energy Flux Anomalies

Anomalies in the individual components of the surface energy balance are shown for El Niño (left column of Figure 2) and for La Niña (right column of Figure 2). We adopt a sign convention in which contributions to positive (negative) local temperature tendency are plotted in red (blue). The effect of changes in the upward longwave radiation merely

represents the radiative response to the anomalous surface temperature itself following the Stefan-Boltzmann law. Thus, temperature tendencies induced by upward longwave flux anomalies are out-of-phase with the composite surface temperature anomalies although the land surface emission may not be perfectly represented as a blackbody emission (compare Figure 1 with top panels of Figure 2).

The surface radiative heating, defined as the sum of absorbed surface net shortwave radiation flux and the downward surface longwave radiation flux, provides a more insightful indication of how water vapor and cloud feedbacks determine the U.S. surface temperature anomalies during ENSO. It is clear from the second row panels in Figure 2 that the patterns of observed temperature anomalies during El Niño and La Niña are almost entirely determined by the surface radiative heating. Note that over the northern U.S., the large positive anomalies of surface radiative heating agree well with the large warm temperature anomalies. Similarly, over the southern U.S., the small negative anomalies of surface radiative heating are in accord with the weak cold temperature anomalies (Figure 2b and Figure 1a). The change in the surface net radiation, which is the sum of the anomalous upward surface longwave radiation and anomalous surface radiative heating, is a small residual resulting from a cancellation of these two components.

We use the ERA-40 reanalysis to estimate the composite anomalies for sensible and latent heating, the results of which are shown in the bottom panels of Figure 2. Despite the independent sources of information for the radiative and turbulent heat fluxes, a broad

compensation between net surface radiation and turbulent heat fluxes (LH+SH), as demanded by Equation (2), is evident. The mis-match in spatial pattern between radiative and turbulent fluxes in some regions is mostly due to the discrepancy in net radiative flux between ERA-40 reanalysis and ISCCP data, since the spatial pattern of net radiative flux of ERA-40 data has a better match with that of the turbulent fluxes shown in Figure 2. Although the pattern of net radiative flux of ERA-40 data is largely consistent with that of ISCCP data, the magnitude of dominant positive anomalies during El Niño and dominant negative anomalies during La Niña as noted in ISCCP data is somewhat underestimated in ERA-40 data.

The energy flux due to phase changes of snow to liquid water is estimated to be much smaller than the turbulent fluxes. Based on the available NARR data, the energy flux due to snow melting is 0.09 W/m^2 during El Niño events averaged over the Pacific Northwest regions, and is 0.1 W/m^2 during La Niña events over the Central U.S. regions. These values are an order of magnitude less than other terms in the energy balance for both phases of ENSO.

The role of clouds, water vapor and land surface feedbacks in determining the pattern of U.S. surface temperature anomalies during ENSO can be inferred from a diagnosis of the two components of surface radiative heating—the absorbed shortwave radiation and the downward longwave radiation. Figure 3 shows the response of the absorbed shortwave radiation (top row), which is the sum of the reflected (upward) surface shortwave radiation (second row) and the incident downward shortwave radiation (third

row). During El Niño winters, a warming contribution due to increased absorbed solar radiation over the northwestern U.S. is the result of two physical processes: a reduction in surface albedo due to snow cover loss (see Figure 4) and increased incoming solar radiation due to a reduction in cloud optical thickness with the former process dominating (Figure 3, fourth row). During La Niña winters, a contribution to cooling by the reduction in absorbed shortwave radiation over the far Northwest U.S. (Figure 3, top right) is mainly the result of increased cloud optical thickness (Figure 3, fourth row right). Over the Southern U.S., a cooling (warming) during El Niño (La Niña) by the decreased (increased) absorbed shortwave radiation is mainly due to the increase (reduction) in cloud optical thickness.

The response of total cloud cover is consistent with that of cloud optical thickness over the northwest and southwest (not shown), but over the Southern U.S., the response of total cloud cover is out-of-phase with that of cloud optical thickness especially for El Niño winters. As noted by Boer (1993), the response of cloud optical depth could be out-of-phase with that of cloud cover in some regions and may play a more important role in regulating the incoming solar radiation. This suggests that the increase (reduction) in cloud optical thickness outweighs the reduction (increase) in cloud cover in the Southern U.S. and that in general, the role of cloud optical thickness is dominant in regulating the incoming solar radiation over the United States during ENSO events.

The physical processes determining the surface radiation anomalies are closely linked to air motions and advection in the free atmosphere. In particular, clouds are a

consequence of vertical air motions and horizontal moisture transport. Figure 3 (bottom) shows the convergence of the vertically integrated water vapor transport in the atmosphere. Clearly, there is a strong spatial agreement between the convergence (divergence) of the atmospheric water vapor transport and the increase (decrease) of cloud optical thickness (Figure 3 fourth row) with the latter being the primary driver of the anomalous downward shortwave radiation.

3.3. Composite Surface Property Anomalies

Anomalies in land surface properties are an important element in understanding land surface temperature anomalies themselves, and also in understanding the asymmetry of those anomalies between El Niño and La Niña (see Figure 1). A key feature is the general decrease in surface albedo over the U.S. during both phases of ENSO (Figure 4, top). This is largely related to snow cover reduction over the northern-central U.S. during El Niño, and mainly over the central U.S. during La Niña (Figure 4, second row). When marginally snow covered areas are initially warmed, for example, through increased downward shortwave radiation (see Figure 3) or increased downward longwave radiation (see Figure 5), snow is apt to melt, lowering the albedo which in turn can cause a positive temperature-snow feedback. Soil moisture changes associated with precipitation anomalies (lower rows of Figure 4) appear to play a role in the surface temperature response through effects on surface albedo also. Increased (decreased) surface albedo over the Southern U.S. is associated with increased (decreased) precipitation and soil moisture during El Niño (La Niña).

The relationship implied in Figure 4 appears contrary to the observational indication that sand and soils exhibit reduced albedo when wet (e.g. Twomey et al. 1986). To further explore the cause of changes in surface albedo, we have used the Global Inventory Modelling and Mapping Studies (GIMMS) Normalized Difference Vegetation Index (NDVI) data sets (Tucker et al. 2005) to examine the response of surface vegetation during El Niño and La Niña winters (not shown). The areas of increased "greenness" over the Northern Plains during El Niño and over the Central Plains during La Niña are consistent with our prior analysis of reduced surface albedo, a reduction that we attributed to the loss of snow cover in each region (see Figure 4). Less clear is the relationship in the southern U.S. mainly covered by Evergreen Forest (Notaro et al. 2006), a small increase in "greenness" is found both during El Niño and La Niña, which would imply a reduction in surface albedo. It should be noted however, that the change in surface albedo is quite small over the Southern US and the upward shortwave radiation anomalies in the Southeastern US associated with albedo changes are a small contribution to the surface energy balance along the Gulf Coast.

3.4 Impact of Precipitable Water on Downward Longwave Radiation

The other key radiative forcing that determines the land surface temperature anomalies during ENSO is the anomalous downward longwave radiation (Figure 5, top). In several areas of the U.S., its amplitude exceeds that of the anomalous absorbed shortwave radiation (see Figure 3, top), most notably in vicinity of the Canadian border, and also over the Southwest U.S. during La Niña. Changes in atmospheric water vapor content are the principal source for the anomalous downward longwave radiation, as is readily

apparent from the very close spatial agreement between the anomalous precipitable water (Figure 5, middle) and the downward longwave radiation (Figure 5, top). During El Niño, an almost continent-wide increase in atmospheric water vapor contributes to an elevated greenhouse effect (e.g. Zhang and Sun 2008) and a forcing of surface temperature warming through the resulting change in downward longwave radiation. Note once again that the anomalous longwave forcing of surface temperature during El Niño is not equal and opposite to that during La Niña, thus further contributing to the asymmetry in the respective surface temperature anomaly patterns above and beyond that resulting from snow-albedo feedbacks.

The column precipitable water anomalies are best understood from the free atmospheric temperature anomalies, rather than from the atmospheric water vapor transport. Clearly, the diagnostics of the vapor flux convergence presented in Figure 3 cannot explain the pattern of column precipitation water vapor anomalies (Figure 5 middle panels). To clarify the cause of the column precipitable water response, we analyzed the free atmosphere column temperature anomalies (1000 hPa-100 hPa), the result of which is shown in Figure 5 (bottom). The anomalies in column mean temperature are quite similar to the anomalies in mid-tropospheric heights during El Niño and La Niña, which together describe the Tropical-Northern Hemisphere (TNH) teleconnection pattern. The analysis reveals that anomalies in column precipitable water (Figure 5, middle panels) are largely consistent with increased (decreased) water vapor holding capacity in regions of tropospheric warming (cooling).

Furthermore, we note that the pattern of precipitable water change is mostly opposite to the change in precipitation itself (see Figure 4, bottom). Areas of increased (reduced) total column water vapor generally experience reduced (increased) winter precipitation, suggesting that the mechanism for precipitation responses to ENSO is intimately linked to the dynamics of weather systems, frontal boundaries, and the phenomena responsible for inducing adiabatic vertical motions and mass convergence, and not merely to the water vapor abundance itself.

4. Discussion

4.1 Synthesis

An observational analysis of the surface energy budget was presented in order to identify the major contributors to the U.S. surface temperature anomalies during ENSO. The study focused on the composite anomalies of water vapor, clouds and land surface properties in order to provide an understanding of the physical processes that shape the regional U.S. wintertime surface temperature anomaly patterns during El Niño and La Niña.

Surface energy balance requires that anomalies in surface radiative heating (defined as the sum of absorbed solar radiation and downward longwave radiation) be balanced by the upward longwave radiation and the net turbulent flux (the sum of latent and sensible heat fluxes). Over land in particular, the change in surface radiative heating is the dominant physical mechanism for determining the response of U.S. surface temperature. As a summary of the physical processes associated with the U.S. ENSO response, Table

2 presents the principal radiative forcings averaged geographically over the largest surface temperature signals. The numbers in brackets indicate the sign agreement of the individual cases and provide a measure for the robustness of the results. During El Niño, strong Northern U.S. warming and Gulf Coast cooling result from increased and reduced surface radiative heating, respectively. The Northern U.S. warming is mainly attributed to increased downward longwave radiation and a reduced reflection of solar radiation which are linked to increased precipitable water and decreased snow cover, respectively. The Gulf Coast cooling is mainly due to the reduction in incident solar radiation resulting from increased cloud optical thickness. During La Niña, strong central and southern U.S. warming likewise results from increased surface radiative heating. Warming over the central U.S. is largely determined by a reduced reflection of solar radiation, owing to snow cover loss. Warming over the Gulf Coast is mainly due to increased incident solar radiation associated with reduced cloud optical thickness, and also due to increased downward longwave radiation associated with a column increase in precipitable water.

Figure 6 further summarizes our principal findings of the main physical processes that explain the U.S. surface temperature responses to ENSO forcing. Shown are anomalies in precipitable water (top panel), cloud optical thickness (second panel), surface temperature (third panel), and surface albedo (bottom panel). The diagram, which synthesizes our results in a quantitative way, highlights the interplay among various features of the hydrological cycle and their ultimate effects on surface temperature. In particular, our analysis reveals that the patterns of surface albedo and cloud optical thickness changes are highly congruent, and that each is further linked to patterns of anomalous

precipitation. During El Niño, dynamical processes tied to storm track shifts (e.g. Held et al. 1989, Hoerling and Ting 1994; May and Bengtsson 1998) result in below normal precipitation over the northern and western U.S. (see Figure 4), and the implied reduced upward vertical motion results in reduced cloud optical thickness (second row), acting to warm surface temperature (third row). This radiatively forced warming combines with reduced precipitation to reduce snow cover over the same region, thereby acting to amplify the surface warming. A similar interplay of physical processes occurs across the central U.S. during La Niña. Precipitation is broadly reduced over the central Great Plains. The anomalous La Niña teleconnections pattern is associated with storm tracks shifted northward to the Canadian border leading to reduced upward motion and reduced cloud optical thickness. The resultant surface warming is amplified by the accompanying loss in snow cover.

The pattern of precipitable water (top row), which further drives surface temperature through water vapor feedbacks, is largely in phase with the overall temperature anomaly itself (third row). During El Niño, greater (lesser) atmospheric water vapor content over the northern (southern) U.S. is consistent with a vertically averaged tropospheric warming (cooling) associated in part with anomalous descent (ascent). These regions of tropospheric warming (cooling) have greater (lesser) water holding capability. A similar argument pertains to the relation between column precipitable water and atmospheric dynamics during La Niña. There is thus a strong coupling between downward longwave radiative flux, as implied by the sign of precipitable water anomalies, and the dynamically driven changes in precipitation itself. In total, based on diagnosis of both

shortwave and longwave radiation, our analysis of the physical processes responsible for the U.S. surface temperature response to ENSO indicates a strong link with dynamical processes that determine vertical motion and precipitation.

The surface temperature anomalies during ENSO integrate the *immediate effects* of physical processes inherent in the energy balance with the *ultimate causal effects* linked to the free atmospheric teleconnections. Our analysis reveals two processes providing this linkage: First, there exists a strong connection between the convergence of the atmospheric water vapor transport, which largely results from the storm track shifts during ENSO, and the cloud optical thickness. The latter affects the downward shortwave radiation, a key contributor to the surface energy balance. Second, the ENSO generated TNH-like teleconnection pattern and related tropospheric column temperature control the column precipitable water and the resulting changes in downward longwave radiation, a second major contributor to the surface energy balance. Changes in land surface properties, especially snow cover, amplify the surface temperature anomalies.

4.2. Concluding Remarks

Our results have implications for the modeling and prediction of U.S. surface temperature anomalies during ENSO. Increasingly, such predictions are produced using dynamical models (e.g. Barnston et al. 2010). Whereas climate models have been extensively validated as to their dynamical attributes regarding responses to ENSO (e.g. storm tracks, teleconnections), little is known about the fidelity of physical processes associated with the surface temperature response in models. It is evident from the results

presented here that the latter is intimately tied to processes of water vapor, clouds, and surface properties, most of which require parameterization in atmospheric models. It is plausible to conceive, in fact likely to be the case, that different climate models may produce very similar teleconnection responses to ENSO forcing, yet render different U.S. surface temperature anomalies, either in amplitude and/or in pattern, owing to uncertainties in parameterizing the hydrologic cycle. In principle, our results suggest that accurate teleconnections will not guarantee accurate surface temperature signals (or predictions), to the extent that representation of key physical processes is deficient. In so far as ENSO is the primary source of U.S. surface temperature predictability, it is evident that a commensurate effort to evaluate the physics of the temperature response be pursued to assess the suitability of climate models for such predictions as has previously been done for the dynamics of teleconnections (Kumar et al. 1996).

Our observational findings have presented a relatively detailed picture for understanding the physics of the U.S. surface temperature response to SST forcing, which may be useful for climate model validation used in seasonal forecasting, and may also serve as a stepping stone for understanding the U.S. surface temperature response to anthropogenic greenhouse gas forcing in nature and in models used for climate change projections.

Acknowledgments

This research was supported by NOAA Climate Program Office. De-Zheng Sun was supported by NSF Climate Dynamics Program under ATM 0553111 and ATM 0852339. The leading author would like to thank Dr. Yuanchong Zhang for helpful discussions.

References

Barnston, A., S. Li, S. Mason, D. DeWitt, L. Goddard, and X. Gong, 2010: Verification of the First 11 Years of IRI's Seasonal Climate Forecasts. *J. App. Met. And Clim*., 49, 493-520.

Boer, G. J., 1993: Climate change and the regulation of the surface moisture and energy budgets. *Climate Dyn.,* **8,** 225–239.

Chahine, M. T., 1992: The hydrological cycle and its influence on climate. *Nature,* 359, 373–380.

Held, I. M., S. W. Lyons, and S. Nigam, 1989: Transients and the extratropical response to El Niño. *J. Atmos. Sci.*, **46**, 163–174.

Hoerling, M. P. and M. Ting, 1994: On the organization of extratropical transients during El Niño. *J. Climate*, **7**, 745–766.

Hoerling M. P., A. Kumar, and M. Zhong, 1997: El Niño, La Niña, and the nonlinearity of their teleconnections. *J. Climate*, 10, 1769–1786.

Hoerling, M. P., and A. Kumar, 2000: Understanding and Predicting Extratropical Teleconnections Related to ENSO. Chapter 2 (pp 57-88) in "*El Niño and the Southern Oscillation: Multi-scale Variability, and Global and Regional Impacts* [eds. H. Diaz and V. Markgraf], Cambridge University Press, 496 pp.

Kalnay, E., et al., 1996: The NCEP/NCAR 40-year reanalysis project, *Bull. Am. Meteorol. Soc*., 77, 437–471.

Kiladis, G. N., and H. Diaz, 1989: Global climatic anomalies associated with extremes in the Southern Oscillation. *J. Climate,* **2,** 1069–1090.

Kumar, A., M. Hoerling, M. Ji, A. Leetmaa, and P. Sardeshmukh, 1996: Assessing a GCM's suitability for making seasonal predictions. *J. Climate*, **9**, 115–129.

Larkin, N. K., and D. E. Harrison, 2005: On the definition of El Niño and associated seasonal average U.S. weather anomalies, Geophys. Res. Lett., 32, L13705, doi:10.1029/2005GL022738.

Lau, N.C., A. Leetmaa, and M.J. Nath, 2008: Interactions between the Responses of North American Climate to El Niño–La Niña and to the Secular Warming Trend in the Indian–Western Pacific Oceans. *J. Climate*, **21**, 476–494.

May, W. and L. Bengtsson, 1998: The signature of ENSO in the Northen Hemisphere midlatitude seasonal mean flow and high-frequency intraseasonal variability. *Meteor. Atmos. Phys*, **69**, 81–100.

Mesinger F., Coauthors, 2006: North American Regional Reanalysis. *Bull. Amer. Meteor. Soc.*, 87, 343–360.

Notaro, M., Z. Liu, and J. W. Williams, 2006: Observed vegetation–climate feedbacks in the United States. *J. Climate*, **19**:763–786.

Quan, X., M. P. Hoerling, J. Whitaker, G. Bates, and T. Xu, 2006: Diagnosing sources of U.S. seasonal forecast skill. *J. Climate*, **19**, 3279-3293.

Ramanathan, V., P. J. Crutzen, J. T. Kiehl, and D. Rosenfeld, 2001: Aerosol, climate and the hydrological cycle, Science, 294, 2119–2124.

Ropelewski C. F., and M. S. Halpert, 1986: North American precipitation and temperature patterns associated with the El Niño/Southern Oscillation (ENSO). *Mon. Wea. Rev.*, 114, 2352–2362.

Ropelewski, C. F., and M. S. Halpert, 1987: Global and regional scale precipitation

patterns associated with the El Niño/ Southern Oscillation. *Mon. Wea. Rev.,* **115,** 1606–1626.

Rossow, W. B., A. W. Walker, D. E. Beuschel, and M. D. Roiter, 1996: International Satellite Cloud Climatology Project (ISCCP) documentation of new cloud datasets, Rep. WMO/TD-737, 115 pp., World Meteorol. Organ., Geneva, Switzerland.

Soden B. J., 2000: The sensitivity of the tropical hydrological cycle to ENSO. *J. Climate*, 13, 538–549.

Sun, D.-Z., J. Fasullo, T. Zhang, and A. Roubicek, 2003: On the Radiative and Dynamical Feedbacks over the Equatorial Pacific Cold Tongue. *J. Climate*, 16, 2425–2432.

Sun, D.-Z., T. Zhang, C. Covey, S. Klein, W. Collins, J. Hack, J. Kiehl, G.A. Meehl, I. Held, and M. Suarez, 2006 : Radiative and Dynamical Feedbacks Over the Equatorial Cold-tongue: Results from Nine Atmospheric GCMs. *J. Climate* , 19, 4059-4074.

Sun, D.-Z., Y. Yu, and T. Zhang, 2009: Tropical Water Vapor and Cloud Feedbacks in Climate Models: A Further Assessment Using Coupled Simulations. *J. Climate*, **22**, 1287-1304.

Trenberth, K. E., 1997: Using atmospheric budgets as a constraint on surface fluxes. *J. Climate*, 10, 2796-2809.

Trenberth, K. E., G. W. Branstator, D. Karoly, A. Kumar, N.-C. Lau, and C. Ropelewski, 1998: Progress during TOGA in understanding and modeling global teleconnections associated with tropical sea surface temperatures, *J. Geophys. Res.*, 103(C7), 14,291–14,324.

Tucker, C. J., J. E. Pinzon, M. E. Brown, D. A. Slayback, E. W. Pak, R. Mahoney, E. F. Vermote and N. El Saleous, 2005: An Extended AVHRR 8-km NDVI Dataset Compatible with MODIS and SPOT Vegetation NDVI Data. *International Journal of Remote Sensing,* 26, 4485–4498.

Twomey, S. A., C. F. Bohren, and J. L. Mergenthaler. 1986: Reflectances and albedo differences between wet and dry surfaces. Appl. Opt., 25, 431–437.

Uppala, S. M., et al., 2005: The ERA-40 reanalysis, *Q. J. R. Meteorol. Soc*., 131, 2961–3012, doi:10.1256/qj.04.176/.

Wang, Z., C.P. Chang, and B. Wang, 2007: Impacts of El Niño and La Niña on the U.S. Climate during Northern Summer, *J. Climate*, **20**, 2165–2177.

Wild, M., A. Ohmura, H. Gilgen, and D. Rosenfeld, 2004: On the consistency of trends in radiation and temperature records and implications for the global hydrological cycle, *Geophys. Res. Lett.,* 31, L11201, doi:10.1029/2003GL019188.

Xie P. P, and P. A Arkin, 1997: Global precipitation: A 17-year monthly analysis based on gauge observations, satellite estimates, and numerical model outputs. *Bull. Amer. Meteor. Soc.*, 78, 2539–2558.

Yang F., A. Kumar, W. Wang, H.-M. H. Juang, and M. Kanamitsu, 2001: Snow–albedo feedback and seasonal climate variability over North America. *J. Climate*, **14**, 4245–4248.

Zhang, Y., W. B. Rossow, A. A. Lacis, V. Oinas, and M. I. Mishchenko, 2004: Calculation of radiative fluxes from the surface to top of atmosphere based on ISCCP and other global data sets: Refinements of the radiative transfer model and the input data, *J. Geophys. Res*., 109, D19105, doi:10.1029/2003JD004457.

Zhang, T., and D.-Z. Sun, 2006: Response of water vapor and clouds to El Niño warming in three National Center for Atmospheric Research atmospheric models, *J. Geophys. Res.*, 111, D17103, doi:10.1029/2005JD006700.

Zhang, T., and D.-Z. Sun, 2008: What causes the excessive response of clear-sky greenhouse effect to El Nino warming in Community Atmosphere Models? J. *Geophys. Res.,* 113, D02108, doi:10.1029/2007JD009247.

Table captions

Table 1: List of warm and cold events from the observational datasets used in the composite analysis.

Table 2: The responses of surface temperature and the associated surface radiative fluxes and surface albedo averaged over the Pacific Northwest (120^{O} W-90^{O} W, 40^{O} N-53^{O} N) and the Gulf Coast (112^{O} W-80^{O} W, 30^{O} N-36^{O} N) for El Niño and over the Central U.S. (120^{O} W-90^{O} W, 37^{O} N-45^{O} N) and the Gulf Coast (112^{O} W-80^{O} W, 30^{O} N-36^{O} N) for La Niña. The values for the responses are obtained based on the composites of 6 (4) warm (cold) cases in Table 1. The numbers in parentheses indicate how much cases yield positive values ("p") and how much cases yield negative values ("n") among those 6 (4) warm (cold) cases concerned. The meanings of symbols are below: "SFCT" indicates "surface temperature", "SRH" surface radiative heating, "LW_dn" downward surface longwave radiation, "SW_dn" downward surface solar radiation, "SW_up" upward surface solar radiation, "SW_net" absorbed solar radiation at surface. Note that here SRH = LW_dn + SW_net = LW_dn + SW_dn +SW_up.

Figure captions

Figure 1**:** Composites of seasonally averaged DJF (December to February) surface temperature anomalies for (a) El Niño and (b) La Niña events. See Table 1 (section 2) for the years used in the composites. Units are ^{O}C.

Figure 2: The composite DJF anomalies of (a) upward longwave radiation, (b) surface radiative heating, (c) net radiation, and (d) the turbulent fluxes for El Niño events. (e–h) Corresponding anomalies of surface energy flux for La Niña events. Units are W/m^2. The surface radiative heating is defined as the sum of the absorbed shortwave and downward longwave radiation at the surface. The net radiation is equal to the sum of surface radiative heating and the upward longwave radiation. The turbulent fluxes are the sum of latent heat flux (LH) and sensible heat flux (SH). Note that energy gain for the surface is signed positive, and energy loss for the surface is signed negative, and provide qualitative indication of their contributions to surface temperature tendency.

Figure 3: The composite DJF anomalies of (a) absorbed shortwave radiation at surface, (b) surface upward shortwave flux, (c) surface downward shortwave flux, (d) cloud optical thickness, and (e) convergence of vertically integrated moisture transport for El Niño events. (f–j) Corresponding anomalies for La Niña events. Units for radiative fluxes are W/m^2, Units for cloud optical thickness are dimensionless, and Units for convergence of vertically integrated moisture transport are mm/day.

Figure 4: The composite DJF anomalies of (a) surface albedo, (b) snow cover, (c) soil moisture content, and (d) precipitation for El Niño events. (e–h) Corresponding anomalies for La Niña events. Units for surface albedo are dimensionless and those for snow cover, soil moisture content and precipitation are %, Kg/m^2, and mm/day, respectively.

Figure 5: The composite DJF anomalies of (a) downward longwave radiation at surface, (b) total column precipitable water, and (c) free atmospheric column temperature (1000 hPa-100 hPa) for El Niño events. (d–f) Corresponding anomalies for La Niña events. Units for radiative fluxes are W/m^2, Units for precipitable water are Kg/m^2, and Units for atmospheric column temperature are ^{O}C.

Figure 6: Schematic diagram showing the physical mechanisms by which the water vapor, clouds, and surface properties (indicated by surface albedo) determine the wintertime surface temperature over the continental United States during ENSO events. Note that contributions to surface warming (cooling) are plotted in red (blue) for water vapor and clouds, and are plotted in black (white) for surface albedo. Reduced surface albedo is indicated by dark shades implying darker surface conditions contributing to warming.

Table 1. List of warm and cold events from the observational datasets used in the composite analysis.

Variable (Symbol)	Dataset	Warm events	Cold events	Reference
Surface radiative fluxes	ISCCP FD	1986/87; 1987/88; 1991/92; 1994/95; 1997/98; 2002/03	1988/89; 1995/96; 1998/99; 1999/2000	Zhang et al. (2004)
Surface temperature, surface albedo and total column precipitable water	ISCCP FD	same as above	same as above	same as above
Cloud amount and cloud optical thickness	ISCCP D2	1986/87; 1987/88; 1991/92; 1994/95; 1997/98; 2002/03	1988/89; 1995/96; 1998/99; 1999/2000	Rossow et al. (1996)
Precipitation	CMAP	1986/87; 1987/88; 1991/92; 1994/95; 1997/98; 2002/03	1988/89; 1995/96; 1998/99; 1999/2000	Xie and Arkin (1997)
Surface latent and sensible heat fluxes (LH and SH)	ERA-40 reanalysis	1986/87; 1987/88; 1991/92; 1994/95; 1997/98	1988/89; 1995/96; 1998/99; 1999/2000	Uppala et al. (2005)
Snow cover and soil moisture content	NARR data	1986/87; 1987/88; 1991/92; 1994/95; 1997/98; 2002/03	1988/89; 1995/96; 1998/99; 1999/2000	Mesinger et al. (2006)
Air temperature	NCEP-NCAR reanalysis	1986/87; 1987/88; 1991/92; 1994/95; 1997/98; 2002/03	1988/89; 1995/96; 1998/99; 1999/2000	Kalnay et al. (1996)
Vertically integrated moisture transport	Trenberth data	1986/87; 1987/88; 1991/92; 1994/95; 1997/98; 2002/03	1988/89; 1995/96; 1998/99; 1999/2000	Trenberth (1997)

ISCCP = International Satellite Cloud climatology Project.
CMAP = CPC Merged Analysis of Precipitation.
ERA-40 = 40-yr ECMWF Re-Analysis.
NARR = North American Regional Reanalysis.
NCEP-NCAR = National Centers for Environmental Prediction–National Center for Atmospheric Research.

Table 2: The responses of surface temperature and the associated surface radiative fluxes and surface albedo averaged over the Pacific Northwest (120^O W-90^O W, 40^O N-53^O N) and the Gulf Coast (112^O W-80^O W, 30^O N-36^O N) for El Niño and over the Central U.S. (120^O W-90^O W, 37^O N-45^O N) and the Gulf Coast (112^O W-80^O W, 30^O N-36^O N) for La Niña. The values for the responses are obtained based on the composites of 6 (4) warm (cold) cases in Table 1. The numbers in parentheses indicate how much cases yield positive values ("p") and how much cases yield negative values ("n") among those 6 (4) warm (cold) cases concerned. The meanings of symbols are below: "SFCT" indicates "surface temperature", "SRH" surface radiative heating, "LW_dn" downward surface longwave radiation, "SW_dn" downward surface solar radiation, "SW_up" upward surface solar radiation, "SW_net" absorbed solar radiation at surface. Note that here SRH = LW_dn + SW_net = LW_dn + SW_dn +SW_up.

Responses to ENSO	El Niño		La Niña	
	Pacific Northwest	Gulf Coast	Central U.S.	Gulf Coast
SFCT (^OC)	1.6 (p: 5 / n: 1)	-0.6 (p: 2 / n: 4)	2.0 (p: 3 / n: 1)	1.4 (p: 4 / n: 0)
SRH (W/m^2)	8.7 (p: 5 / n: 1)	-1.7 (p: 1 / n: 5)	5.6 (p: 3 / n: 1)	10.1 (p: 4 / n: 0)
LW_dn (W/m^2)	4.9 (p: 5 / n: 1)	1.9 (p: 3 / n: 3)	2.2 (p: 3 / n: 1)	3.7 (p: 3 / n: 1)
SW_dn (W/m^2)	0.2 (p: 3 / n: 3)	-3.6 (p: 0 / n: 6)	-1.7 (p: 1 / n: 3)	5.1 (p: 3 / n: 1)
SW_up (W/m^2)	3.6 (p: 6 / n: 0)	0.0 (p: 3 / n: 3)	5.1 (p: 3 / n: 1)	1.4 (p: 4 / n: 0)
SW_net (W/m^2)	3.8 (p: 6 / n: 0)	-3.6 (p: 2 / n: 4)	3.5 (p: 4 / n: 0)	6.4 (p: 3 / n: 1)
Surface Albedo	-0.041 (p: 1 / n: 5)	0.0050 (p: 4 / n: 2)	-0.047 (p: 0 / n: 4)	-0.015 (p: 0 / n: 4)

Figure 1. Composites of seasonally averaged DJF (December to February) surface temperature anomalies for (a) El Niño and (b) La Niña events. See Table 1 (section 2) for the years used in the composites. Units are ^{o}C.

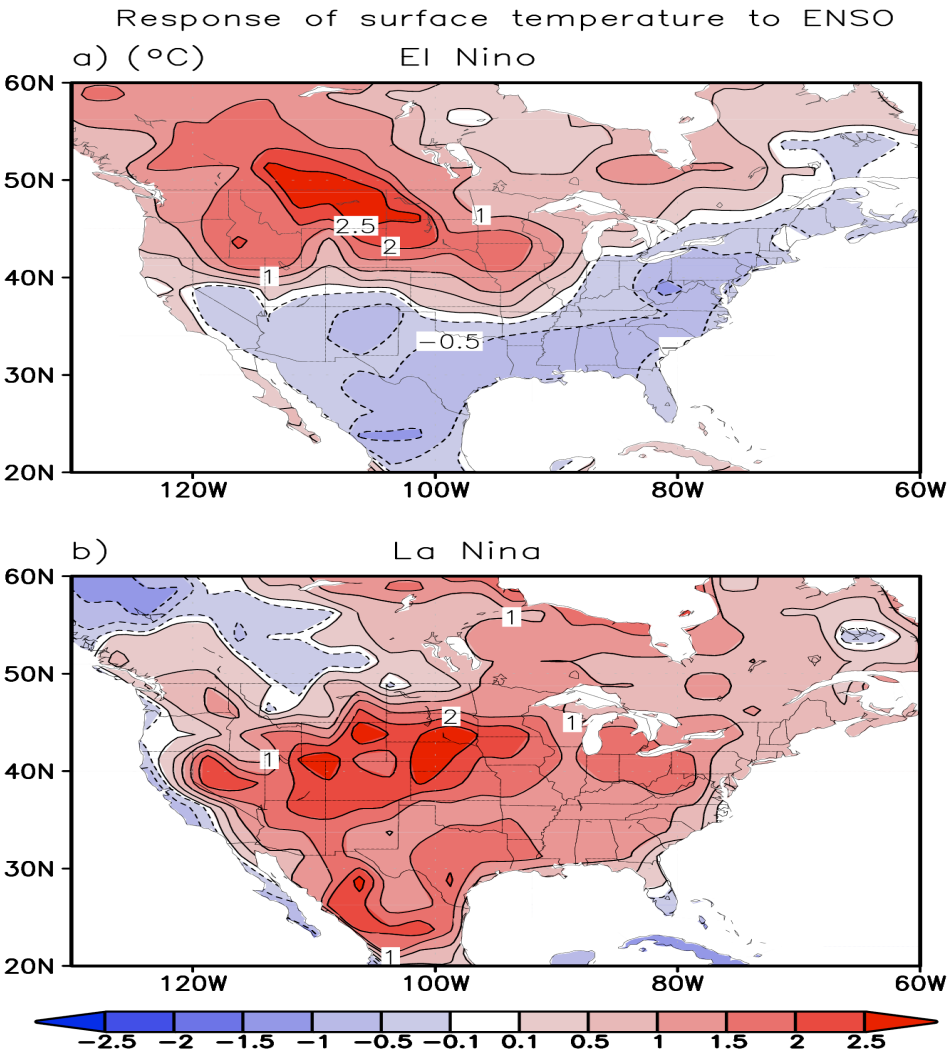

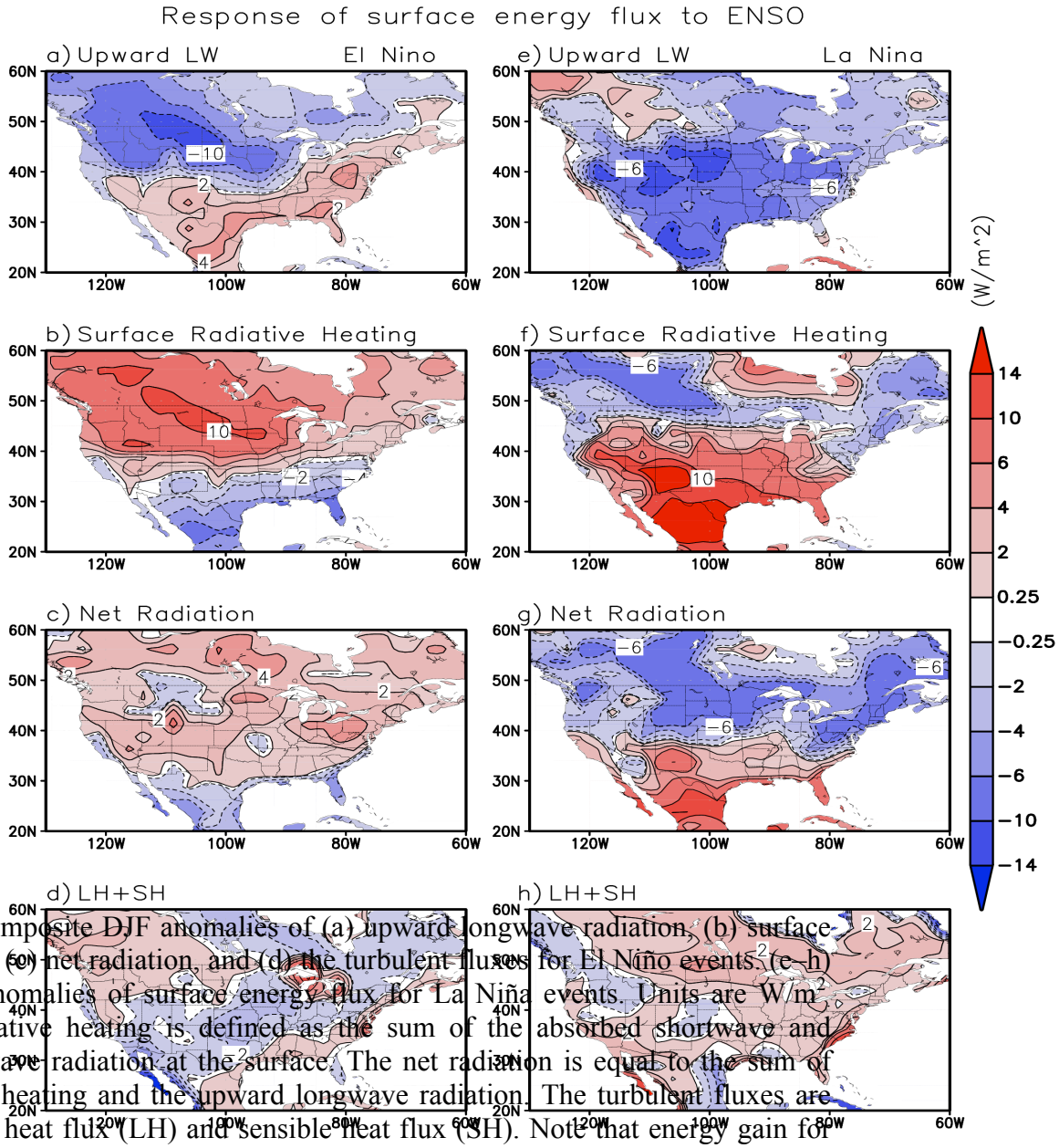

igure 2: The composite DJF anomalies of (a) upward longwave radiation, (b) surface diative heating, (c) net radiation, and (d) the turbulent fluxes for El Niño events. (e–h) orresponding anomalies of surface energy flux for La Niña events. Units are W/m^2. ıe surface radiative heating is defined as the sum of the absorbed shortwave and wnward longwave radiation at the surface. The net radiation is equal to the sum of rface radiative heating and the upward longwave radiation. The turbulent fluxes are e sum of latent heat flux (LH) and sensible heat flux (SH). Note that energy gain for e surface is signed positive, and energy loss for the surface is signed negative, and ovide qualitative indication of their contributions to surface temperature tendency.

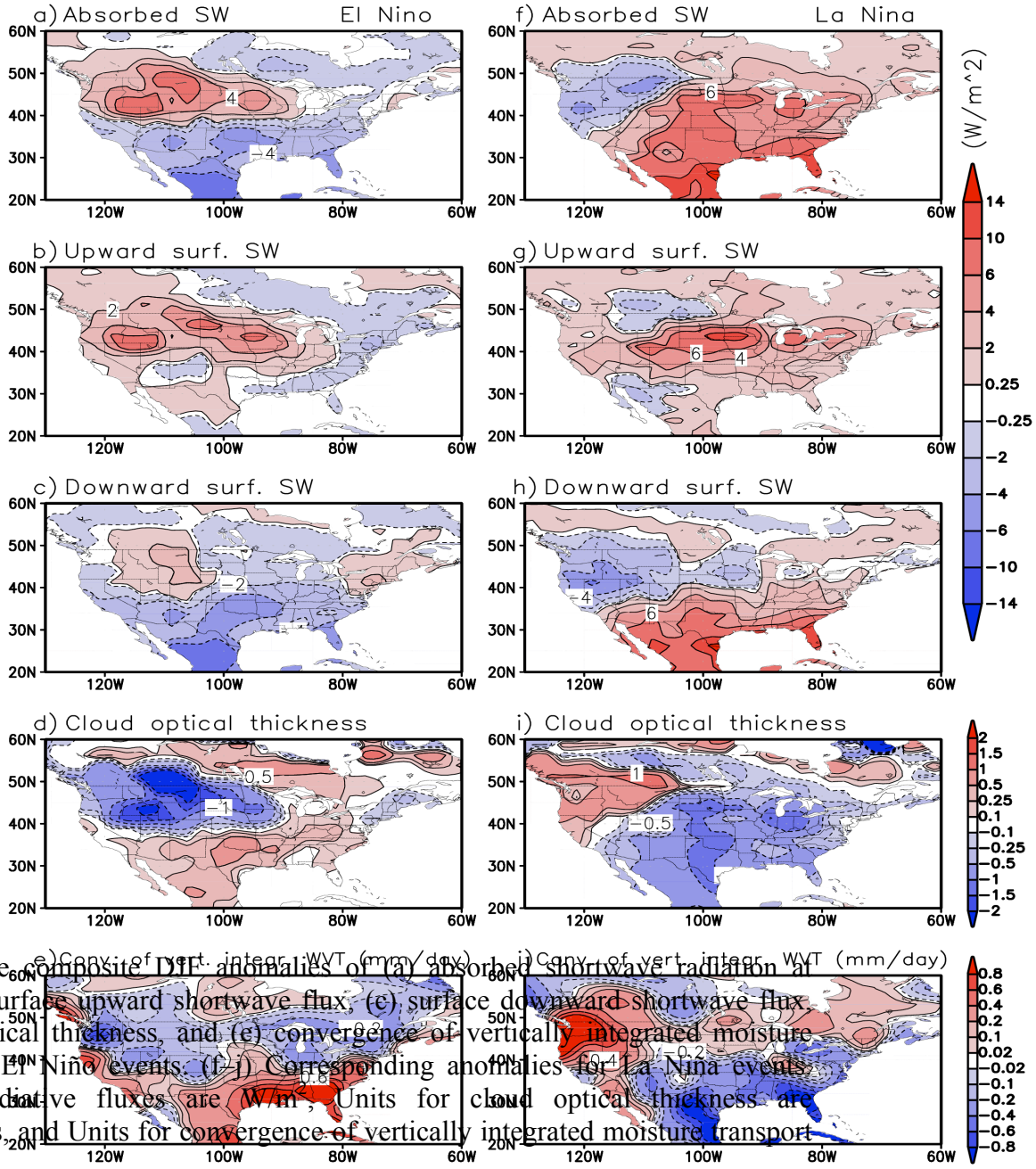

Figure 3: The composite DJF anomalies of (a) absorbed shortwave radiation at surface, (b) surface upward shortwave flux, (c) surface downward shortwave flux, (d) cloud optical thickness, and (e) convergence of vertically integrated moisture transport for El Niño events. (f–j) Corresponding anomalies for La Nina events. Units for radiative fluxes are W/m^2, Units for cloud optical thickness are dimensionless, and Units for convergence of vertically integrated moisture transport are mm/day.

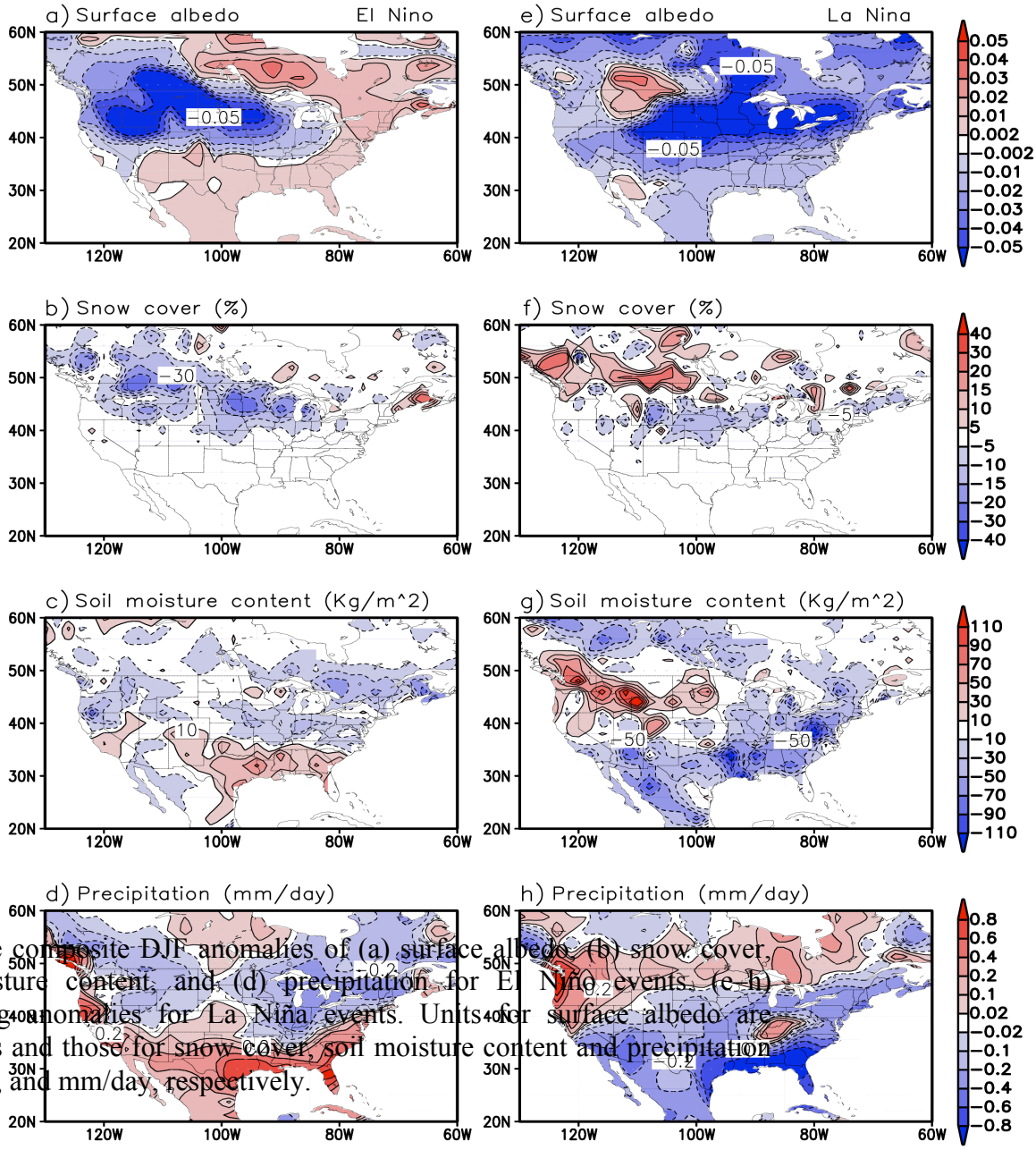

Figure 4: The composite DJF anomalies of (a) surface albedo, (b) snow cover, (c) soil moisture content, and (d) precipitation for El Niño events. (e–h) Corresponding anomalies for La Niña events. Units for surface albedo are dimensionless and those for snow cover, soil moisture content and precipitation are %, Kg/m^2, and mm/day, respectively.

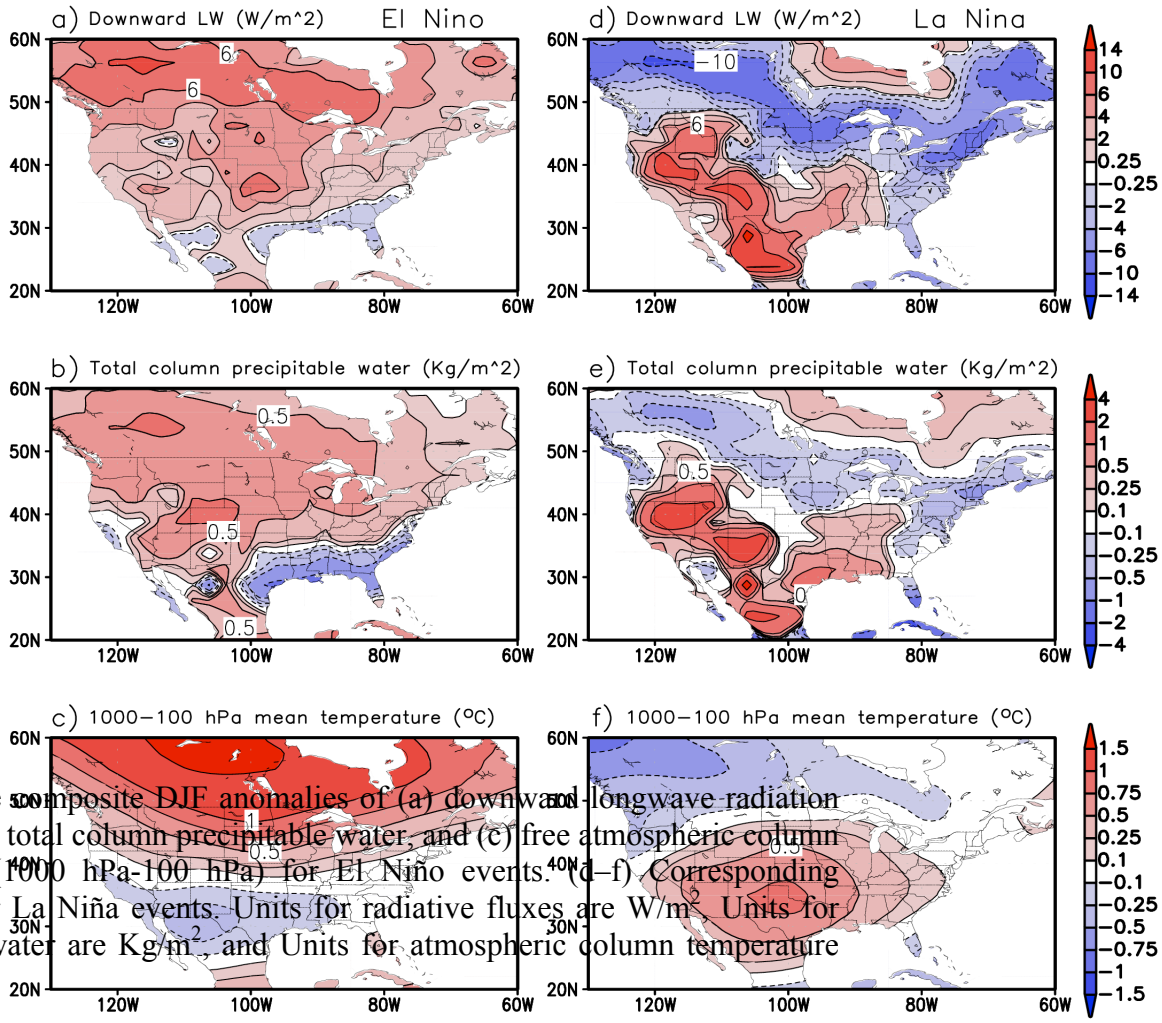

Figure 5: The composite DJF anomalies of (a) downward longwave radiation at surface, (b) total column precipitable water, and (c) free atmospheric column temperature (1000 hPa-100 hPa) for El Niño events. (d–f) Corresponding anomalies for La Niña events. Units for radiative fluxes are W/m^2, Units for precipitable water are Kg/m^2, and Units for atmospheric column temperature are ^oC.

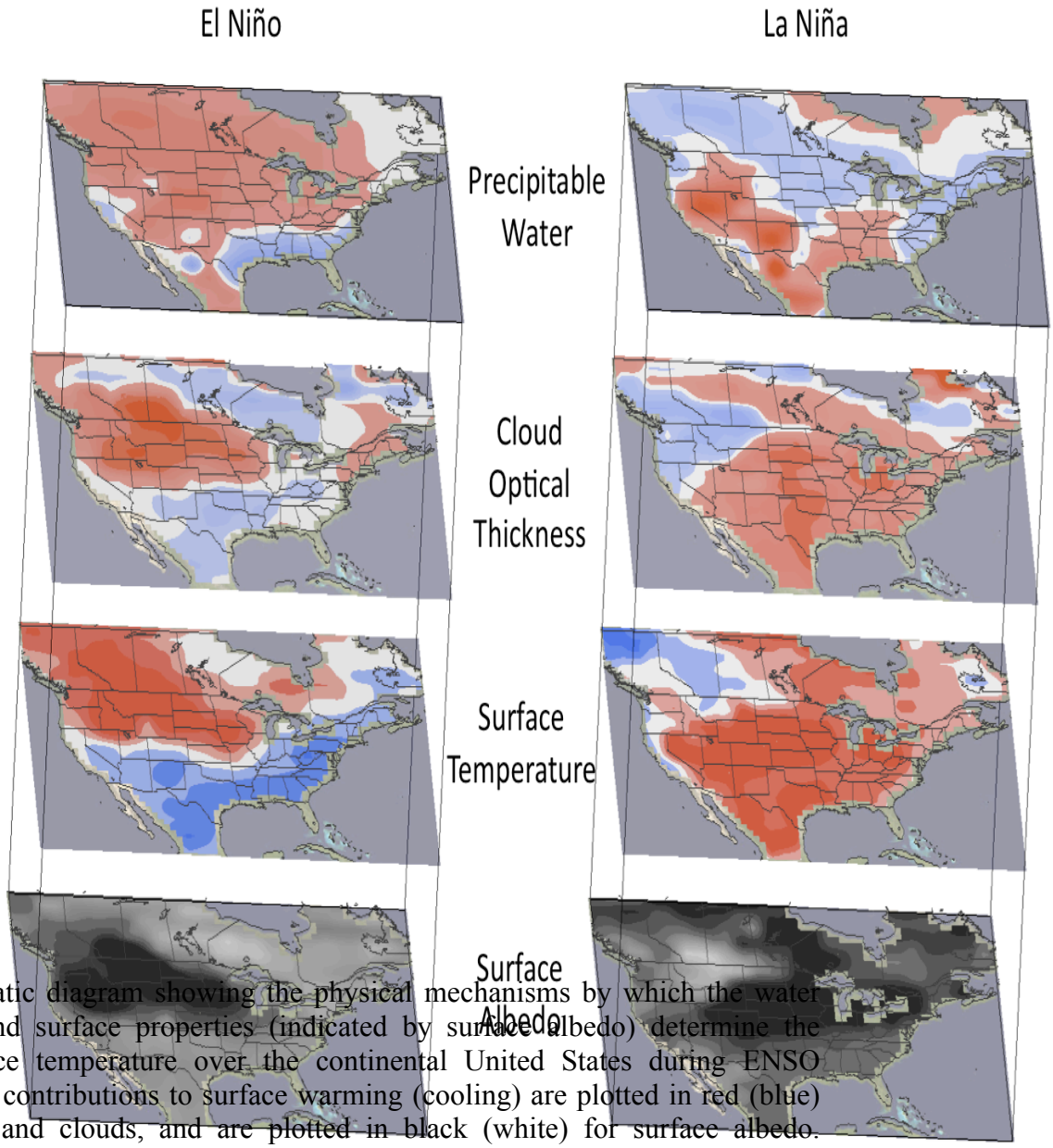

Figure 6: Schematic diagram showing the physical mechanisms by which the water vapor, clouds, and surface properties (indicated by surface albedo) determine the wintertime surface temperature over the continental United States during ENSO events. Note that contributions to surface warming (cooling) are plotted in red (blue) for water vapor and clouds, and are plotted in black (white) for surface albedo. Reduced surface albedo is indicated by dark shades implying darker surface conditions contributing to warming.